




The Mean Temperatures of CME-Related Dimming Masses

Emily Thomson¹ · Hugh Hudson^{1,2} 

Received: 6 October 2023 / Accepted: 26 October 2023 / Published online: 16 November 2023
© The Author(s) 2023

Abstract

Sun-as-a-star EUV spectroscopy from EVE (the Extreme-ultraviolet Variability Experiment, on board SDO, the Solar Dynamics Observatory) frequently shows striking irradiance reductions following major solar flares. These coincide with dimming events as seen in EUV and X-ray images, involving the evacuation of large volumes of the corona by the associated coronal mass ejections. The EVE view of the dimming process is precise and quantitative, whereas difference imaging in the EUV reveals the structures to be full of complicated detail due most likely to unrelated activity. We have studied a sample of 11 events, mostly GOES X-class flares, all of which were associated with coronal mass ejections. For a set of nine lines of Fe ions at stages VIII–XIII, corresponding to nominal peak formation temperatures below $\log(T/K) = 6.3$, we have compared the emission-measure-weighted temperature of the preflare global corona and that of the dimming mass, defined by the deficit at the time of greatest dimming. We find similar temperatures by this measure, but with a distinctly narrower variation in the preflare samples. For higher ionization states, weak emission commonly appears during the dimming intervals, consistent with residual late-phase flare development. The dimming depths do not appear to correlate with the preflare state of the global corona.

1. Introduction

The solar corona undergoes drastic transformations at times of coronal mass ejections, which can “deplete” a substantial sector of the white-light corona (Hansen et al., 1974). These abrupt depletions were identified in Skylab soft-X-ray observations as transient coronal holes, also known as coronal dimmings (Rust, 1983) and show a sudden decrease in brightness in both the soft X-ray (SXR) (Sterling and Hudson, 1997) and extreme-ultraviolet (EUV) (Zarro et al., 1999) wavelength ranges. Coronal dimmings have been found to occur near active regions and typically range from 3 to 12 h, with a sudden drop to the peak dimming and a slow recovery (Reinard and Biesscker, 2008). They can also be identified by irra-

✉ H. Hudson
hugh.hudson@glasgow.ac.uk

E. Thomson
emilyt5150@gmail.com

¹ SUPA School of Physics and Astronomy, University of Glasgow, Glasgow G12 8QQ, UK

² SSL, University of California, Berkeley CA, USA

Table 1 CHIANTI details for an EVE line subset.

Line	Wavelength (Å)	$\log T(\text{K})^*$	$G(T)^*$
Fe VIII	131.24	5.75	1.42×10^{-24}
Fe IX	171.073	5.9	2.96×10^{-23}
Fe X	174.531	6.05	1.34×10^{-23}
Fe X	177.23	6.05	7.66×10^{-24}
Fe X	184.536	6.05	3.30×10^{-24}
Fe XI	180.401	6.10	1.06×10^{-23}
Fe XI	188.216	6.10	5.69×10^{-24}
Fe XII	196.64	6.2	1.35×10^{-24}
Fe XIII	202.044	6.25	2.09×10^{-24}
Fe XIV	274.2	6.3	2.54×10^{-24}
Fe XIV	264.79	6.3	4.65×10^{-24}
Fe XIV	270.519	6.3	1.80×10^{-24}
Fe XIV	211.331	6.3	4.87×10^{-24}
Fe XV	69.682	6.35	8.54×10^{-25}
Fe XV	284.163	6.35	1.84×10^{-23}
Fe XVIII	93.9322	6.85	1.12×10^{-24}
Fe XVIII	103.95	6.85	3.69×10^{-25}
Fe XIX	108.355	6.95	8.68×10^{-25}

*Peak of $G(T)$ function ($\text{erg cm}^{-3} \text{ s}^{-1}$).

diancance measurements from the EUV Variability Experiment (EVE) (Mason et al., 2014) and observations with this instrument found similar dimming durations (Veronig et al., 2021).

The Solar Dynamics Observatory (SDO) (Pesnell, Thompson, and Chamberlin, 2012) has three instruments onboard, one of which is EVE (Woods et al., 2012), used to measure the EUV and SXR spectral irradiance. The data we use come from EVE's Multiple EUV Grating Spectrographs (MEGS), consisting of two spectrographs: MEGS-A, which measures the 5 to 37 nm range, and MEGS-B, which measures the 35 to 105 nm range, both at moderate (1 Å) spectral resolution. These operated from 2010 to 2014, recording a solar spectrum every 10 s. After 2014, only MEGS-B continued to collect data for a reduced amount of time each day but recently with 60-s averages. Table 1 lists our subset of lines observed relatively cleanly (few apparent blends) by EVE. Dimming typically occurs in lines with a formation temperature of $\log(T/\text{K}) = 5.8 - 6.3$; earlier spectroscopic analysis of the differential emission measure (DEM) revealed that the material leaving the corona in a CME is typically in the range $\log(T/\text{K}) = 6.0 - 6.3$ (Tian et al., 2012). Coronal dimmings are important for studying space weather as CMEs can lead to geomagnetic storms that have an impact on various aspects of human society and technology.

This paper aims to help identify the source of the CME mass by examining the emission-measure-weighted mean temperature using the different lines observed by EVE for both the preflare global corona and the dimming mass. We define the dimming mass via the simple background subtraction of the dimmed corona from the preflare corona, and note that this does not reflect the state changes during the dimming process itself. EVE has a unique Sun-as-a-star perspective, whereas all dimming observations by white-light coronagraphs have occulter-height restrictions. We note another distinction here, namely that the EVE emission lines predominantly have emissivity depending basically upon n_e^2 , whereas the Thomson-scattering emissivity as seen by a coronagraph varies as n_e directly.

2. Observations

2.1. Coronal Dimmings

A time-series plot of irradiance values for a particular EVE emission line occasionally displays a prominent dimming feature, recognizable at the full sampling at 10-s cadence but typically lasting for hours. In most cases, a stable pre-event time interval provides a background estimate for the dimming, and a simple subtraction allows us to characterize that part of the pre-event coronal plasma involved in the dimming. The dimming mass thus revealed corresponds to that of the accompanying coronal mass ejection (CME). Note that this observation does not depend upon CME dynamics and is just a description of the depletion of the corona, with the important caveat that flare emissions (excess over background) may compete with the dimming at some wavelengths.

We have selected a subset of the EVE lines, avoiding obviously blended ones so that a simple single Gaussian fit can provide a good determination of the emission measure of the dimming mass. The spectral lines thus chosen are listed in Table 1. The Fe X line at 177.23 Å was chosen for the initial identification process as it invariably shows the dimmings well. The table lists 11 examples, all of which could be identified with CMEs observed by LASCO and with solar flares on the visible hemisphere. This is not a complete sample, but a representative list including events from Mason et al. (2019), plus a series of events associated with X-class flares.

The irradiance values every 10 s over a 12-h period were determined via Gaussian fits for each line and plotted against time, and background and dimming fluxes were measured for each spectral line. To assess uncertainties, a peak dimming time was identified and split into 5-min time intervals. Across each of these intervals, the mean flux and standard error were recorded for analysis. Similarly we defined a background time of 100 min and rebinned to 1-min samples, over which the mean flux and standard error were found. The dimming pattern in the Fe X line for each event, with the time intervals chosen for analysis, can be seen in Figure 1. We also show snapshot difference images for these times, using the AIA 193 Å channel, in Figure 2. Note that these do not show the dimmings very clearly, except for three events at or near the limb itself, where the dimming can be seen clearly to have come from the large-scale corona rather than from the active region in the lower corona specifically.

2.2. Comments on Specific Events

The time series typically show a stable pre-event emission level, a peak at flare time, and the dimming. The flare peak in this line reflects the impulsive phase of the flare, rather than the gradual phase shown by GOES soft-X-ray emissions. We interpret the early Fe X emission as forming at chromospheric heights during the impulsive phase, corresponding to the characteristic nonthermal radio and hard-X-ray emissions (e.g., Hudson et al., 1994). Note that the plots for SOL2012-01-27 and SOL2012-05-17 deviate from this pattern by not having prominent impulsive phases. We expect this behavior in limb events, for which the chromospheric sources may have optical-depth effects or even partial occultation by the limb; this could be thought of as a special case of “obscuration dimming” (e.g., Mason et al., 2014). The difference images tend to bear this out but do not show clean signatures, reflecting coronal activity and solar rotation over the typically several-hour time interval.

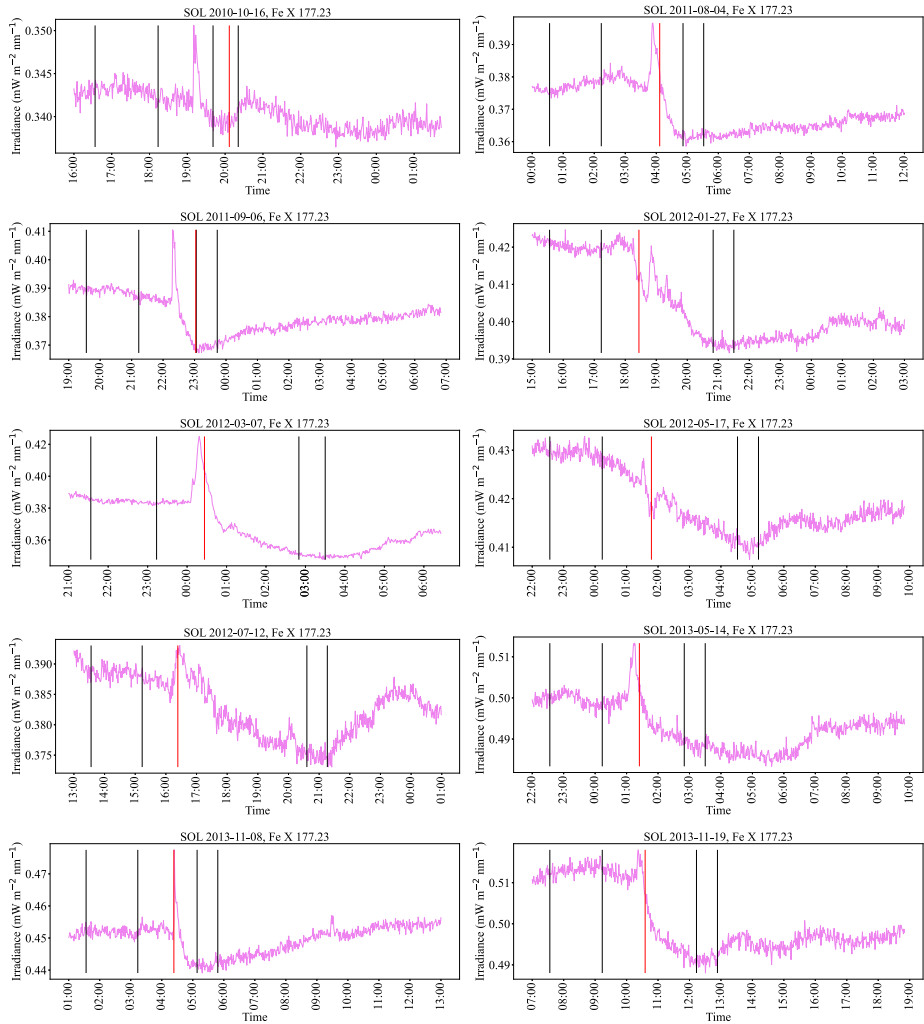


Figure 1 Time series of multiple solar flare events for Fe X 177.23 Å. The background and dimming time intervals used for temperature analysis are indicated by the black vertical lines. The red vertical lines show the time of first detection of the CME, with values provided by the Large Angle and Spectrometric Coronagraph (LASCO) catalog.

2.2.1. SOL2012-03-07

This well-known flare, at X5.7 the most energetic of the events in our sample, also showed the greatest dimming depth in the Fe X reference line, about 12% relative to the preflare level. Table 3 lists the derived values of emission measure from the first 5-min interval of SOL2012-03-07, an exceptionally well-observed event, with Figure 3 showing the background-subtracted spectrum of this interval. This spectrum shows the most useful dimming lines mainly in the range 170–210 Å, but with many flare emission lines as well. These mainly come from higher ionization states than the dimming lines, with the notable exception of the prominent 30.4 nm line of He II. Note that the dimming line Fe X 177.23 Å

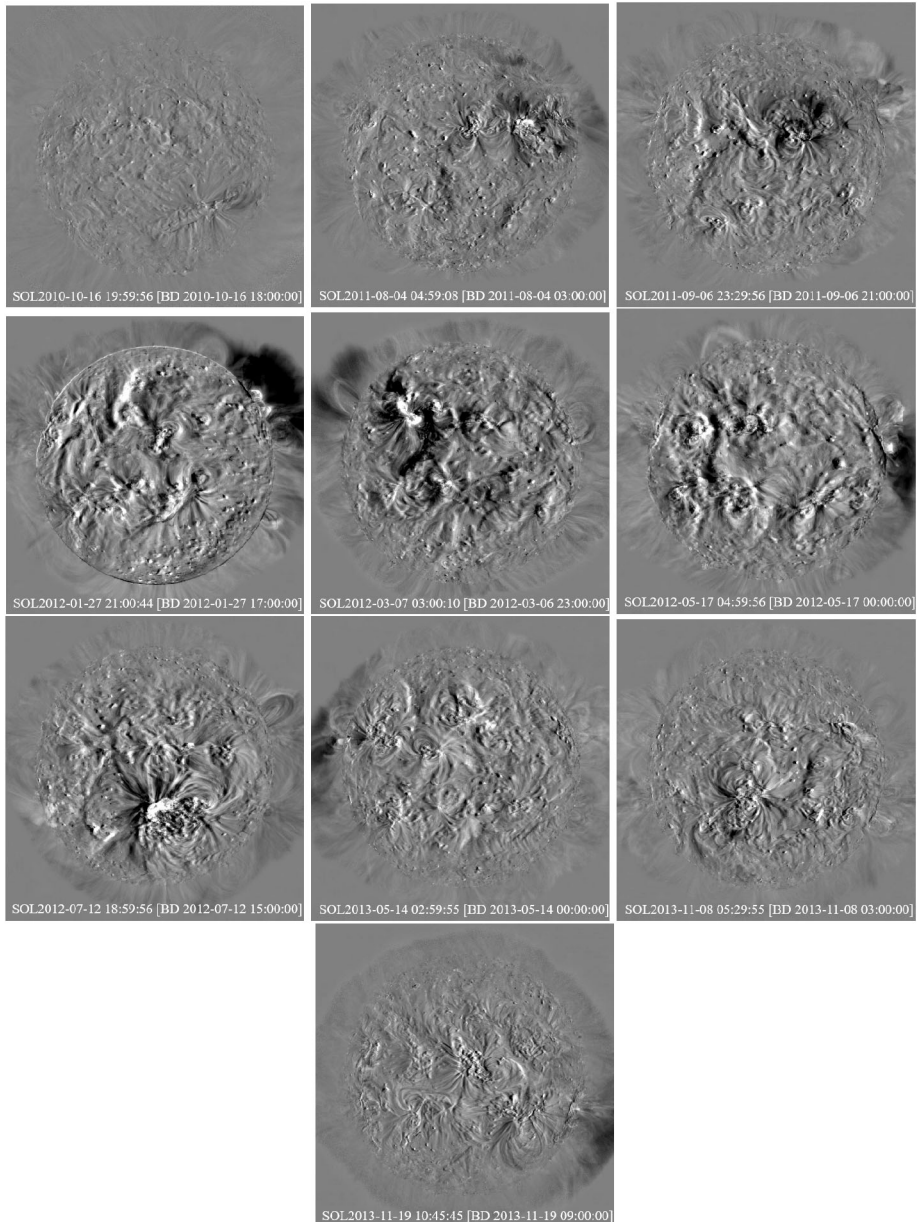


Figure 2 Base-difference images from the preflare background and dimming time created using the 193 Å AIA channel via Heliviewer: left to right, top to bottom, in the order of Table 2. The image and base-difference image times appear on each image.

itself (and many low-excitation lines) goes into emission during the flare-impulsive phase (Figure 1), but over a very limited time range. This spectrum illustrates the great power of the EVE spectra to distinguish event phases with excellent signal-to-noise ratio.

Table 2 List of dimming events and their properties.*

Event ^a	CME (UT)	GOES class	Dimming Fe X, %	Lat ^c (°)	Lon ^c (°)	μ
2010-10-16T19:12	20:12:06	M2.9	3.2	-20	26	0.80
2011-08-04T03:57	04:12:05	M9.3	4.3	16	38	0.78
2011-09-06T22:20	23:05:57	X2.1	5.3	14	18	0.89
2012-01-27T18:37	18:27:52	X1.7	7.0	NA	NA	0.00
2012-03-07T00:24	00:24:06	X5.4	9.7	18	-31	0.77
2012-05-17T01:47	01:48:05	M5.1	4.9	NA	NA	0.00
2012-07-12T16:49	16:24:05	X1.4	3.4	-13	3	0.95
2013-05-14T01:11	01:25:51	X3.2	2.5	NA	NA	0.00
2013-11-05T22:12	22:36:05	X3.3	0.6	-12	-44	0.69
2013-11-08T04:26	03:24:07	X1.1	2.5	-13	-13	0.93
2013-11-19T10:26	10:36:05	X1.0	1.9	-13	69	0.34

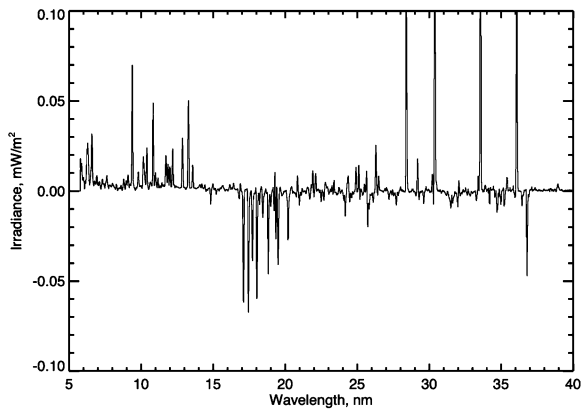
*For the three limb events we set $\mu = 0.00$.

^aTime field specifies GOES 1–8 Å peak time; ^bNOAA; ^cStonyhurst coordinates.

Table 3 Derived values for SOL2012-03-07, 02:30-35 UT.

Line	Wavelength (Å)	Dimming depth ($\times 10^{-6}$ W/m ² /nm)	Preflare emission measure ($\times 10^{18}$ m ⁻⁵)	Dimming emission measure ($\times 10^{18}$ m ⁻⁵)
Fe VIII	131.24	0.978 ± 0.17	1.11 ± 0.0015	0.69 ± 0.082
Fe IX	171.073	-56.0 ± 0.62	0.91 ± 0.0005	-1.89 ± 0.021
Fe X	174.531	-54.9 ± 0.62	2.09 ± 0.0007	-4.09 ± 0.047
Fe X	177.23	-33.8 ± 0.33	2.51 ± 0.0008	-4.41 ± 0.044
Fe X	184.536	-15.3 ± 0.35	3.59 ± 0.0017	-4.64 ± 0.102
Fe XI	180.401	-51.7 ± 0.45	2.78 ± 0.0008	-4.88 ± 0.043
Fe XI	188.216	-38.0 ± 0.41	4.08 ± 0.0011	-6.77 ± 0.073
Fe XII	196.5253	-33.4 ± 0.47	18.5 ± 0.0055	-24.8 ± 0.345
Fe XIII	202.044	-24.3 ± 0.47	10.9 ± 0.0031	-11.7 ± 0.226
Fe XIV	274.2	-2.45 ± 0.39	3.34 ± 0.0024	-0.96 ± 0.152
Fe XIV	264.79	0.697 ± 0.34	1.92 ± 0.0012	0.15 ± 0.073
Fe XIV	270.519	0.409 ± 0.33	2.32 ± 0.0022	0.23 ± 0.182
Fe XIV	211.331	-3.30 ± 0.38	3.36 ± 0.0015	-0.68 ± 0.078
Fe XV	69.682	3.50 ± 0.85	10.9 ± 0.017	4.10 ± 0.993
Fe XV	284.163	63.7 ± 1.13	1.68 ± 0.0013	3.46 ± 0.061
Fe XVIII	93.9322	22.4 ± 0.18	4.16 ± 0.012	20.0 ± 0.164
Fe XVIII	103.95	2.97 ± 0.22	13.8 ± 0.014	8.05 ± 0.604
Fe XIX	108.355	10.5 ± 0.16	3.07 ± 0.0072	12.1 ± 0.190

Figure 3 A representative dimming spectrum, from SOL2012-03-07 at 02:30 UT with the pre-event background subtracted. The dimming lines, notably in the 17–21 nm range, are well separated from residual flare excess lines. These latter are mostly at higher formation temperatures. The four brightest emission lines, clipped at 0.1 mW/m^2 , are Fe XV (28.4163 nm), He II (30.378 nm), and Fe XVI (33.5409 and 36.8071 nm).



2.2.2. SOL2013-11-05T22:12

This event has a poorly determined background level, and our systematic survey distinctly underestimates the dimming magnitude. Many other events occurred on this day, for example SOL2013-11-05T21:13 (C6.9) and an earlier M-class flare. We therefore discard this event from our statistical summaries below.

2.2.3. The Limb Events

Three of our samples (SOL2012-01-27, SOL2012-05-17, and SOL2013-05-14) turn out to have been events at the extreme limb. In the time series (Figure 1) these appear to have wavelength-dependent peculiarities, as mentioned above, but with clearly defined EVE dimming patterns. This shows geometrically that the EVE dimmings actually do show the removal of diffuse coronal plasma, rather than compact low-lying loop systems involved in the eruption. The latter could, in principle, dominate the EM-weighted temperatures of the ejecta, but do not seem to do so; we discuss this in the section below.

The difference images (Figure 2) do not display the dimming so simply as do the Sun-as-a-star EVE time series, owing to apparent motions via solar rotation as well as many image changes due to unrelated magnetic activity, but these limb events do show the phenomenon on this time scale relatively well. The complex temperature responses of the AIA spectral passbands, as compared with the more monochromatic EVE data, may also contribute to this image confusion. See also Jin et al. (2022), who intercompare dimming signatures with AIA images as well as EVE data, and numerical simulations of a different well-studied event, SOL2011-02-15.

2.3. EM-Weighted Mean Temperatures

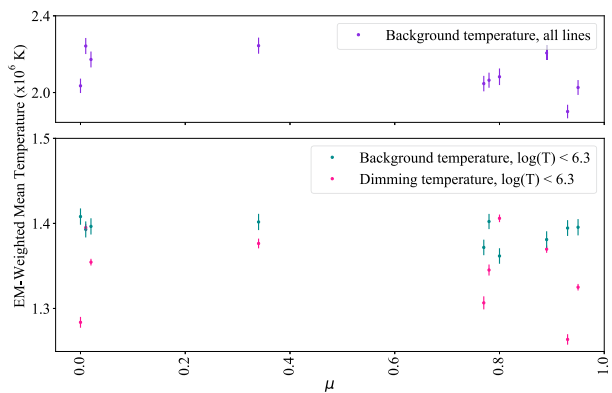
A dimming-mass emission measure for each line can be found by dividing both the preflare background and dimming flux by the line's contribution function, $G(T)$, and subtracting them. The hotter lines do not display dimming, and in fact often go into excess at or above the Fe XIV level ($\log(T/K) = 6.3$) due to late-phase flare emissions. Figure 3 shows these flare-related emission lines clearly as excesses in the difference spectrum. For each event, we calculate an EM-weighted mean temperature $\langle T \rangle$ by using:

$$\langle T \rangle = \frac{\sum_i \frac{T_i \times w_i F_i}{G_i(T_i)}}{\sum_i \frac{w_i F_i}{G_i(T_i)}} , \quad (1)$$

Table 4 EM-weighted mean temperatures for each event.

Event	Dimming material $\log(T/K) < 6.3$ (MK)	Preflare $\log(T/K) < 6.3$ (MK)	Preflare (All) (MK)
SOL2010-10-16	1.41 ± 0.0045	1.36 ± 0.0091	2.08 ± 0.043
SOL2011-08-04	1.37 ± 0.0042	1.39 ± 0.0103	2.22 ± 0.041
SOL2011-09-06	1.37 ± 0.0043	1.38 ± 0.0097	2.21 ± 0.039
SOL2012-01-27	1.40 ± 0.0043	1.39 ± 0.0094	2.24 ± 0.042
SOL2012-03-07	1.35 ± 0.0065	1.40 ± 0.0091	2.06 ± 0.040
SOL2012-05-17	1.35 ± 0.0039	1.40 ± 0.0095	2.17 ± 0.041
SOL2012-07-12	1.32 ± 0.0038	1.40 ± 0.0096	2.03 ± 0.039
SOL2013-05-14	1.28 ± 0.0064	1.41 ± 0.0096	2.04 ± 0.038
SOL2013-11-08	1.26 ± 0.0062	1.39 ± 0.0093	1.90 ± 0.035
SOL2013-11-19	1.38 ± 0.0057	1.40 ± 0.0095	2.24 ± 0.042

Figure 4 The EM-weighted mean temperature for each event, plotted against the cosine of the vertical angle. The purple points display the values for the background time range with all lines included in the calculation. The green and pink points display the background and dimming values, respectively, for lines with a formation temperature $\log(T/K) < 6.3$.



where F_i is the flux, δF_i its uncertainty, and $w_i = F_i/\delta F_i$ the weight for the i th line, with $G_i(T_i)$ the line's contribution function at its temperature peak. For δF_i we use the goodness of fit of the Gaussian parameters for the background time interval. The mean temperature calculated in this way is essentially that of an assumed Gaussian emission-measure distribution.

To quantify the error on the EM-weighted mean temperatures, we used the bootstrap method (e.g., Efron and Tibshirani, 1993). This involves random sampling from the existing flux values of each line to create new samples, from which a temperature can be calculated. The standard error of these temperatures is the estimated error on the EM-weighted mean temperature. Similarly, for each 5-min interval of the dimming flux, the temperature and standard error were found. These can be found in Table 4 and were plotted for each event as seen in Figure 4.

This analysis reveals the temperatures of the dimming masses to be similar to those of the preflare background. Because of confusion with late-phase flare emissions, we have systematically restricted the line list to lines below $\log(T/K) = 6.3$, and note that largest contributor to the overall emission measure of the dimming mass is normally the Fe XII line at 195.12 Å from our line list. Given that active regions dominate this Sun-as-a-star background signal, as shown generally by EUV images, this suggests that the dimming masses

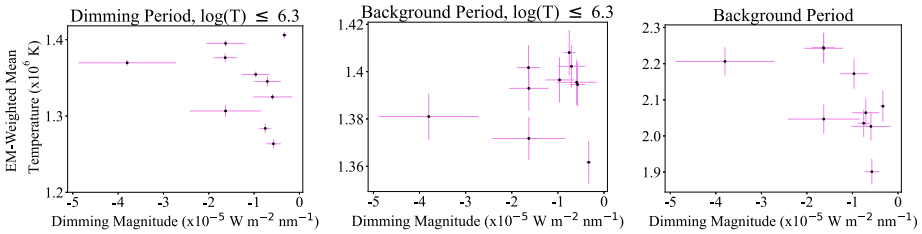


Figure 5 The EM-weighted mean temperatures for the different line ranges against the dimming depth for each event. The average dimming depth across the different lines of each event was used. There is no clear correlation.

Table 5 Pearson correlation coefficient EM-weighted mean temperatures.

Dimming spectrum, $\log(T/K) < 6.3$	0.65
Flare spectrum, $\log(T/K) < 6.3$	-0.35
Flare spectrum, all T	-0.15

originated in the global corona, rather than in the active regions themselves. The lack of a center-to-limb variation (the independence on μ as shown in Figure 4) also supports this conclusion. We also note from Figure 4 that the EM-weighted temperatures differ significantly from event to event, but that they scatter around a well-defined mean value.

The temperatures were also compared with the dimming depth, as seen in Figure 5, for the dimming volume and preflare background of both all the lines and lines with a temperature $\log(T/K) < 6.3$. The peak dimming intensity value was used for each line with the preflare flux subtracted and the average depth and standard error across the lines with $\log(T/K) < 6.3$ was used. Pearson’s correlation coefficient was found for each data set with the results summarized in Table 5. We find no correlation between AR mean temperature and dimming depth.

Figure 4 shows that the preflare corona has a higher mean temperature than those of the dimming masses, using the entire line list. The preflare temperatures also vary significantly. For the restricted line list ($\log(T/K) < 6.3$) the variation is much smaller in the preflare spectra. By contrast, the dimming masses vary significantly, but still within a fairly narrow range: the flare-to-flare values have mean EM-weighted temperature of $1.35 \cdot 10^6$ K, with sample standard deviation 0.05 MK. The dimming-evacuated corona seems to have a rather well-defined temperature by this measure.

3. Does Appreciable CME Mass Come from the Lowest Corona?

A CME, by definition, is only directly observable by a white-light coronagraph, but there are other tools that relate to the process (e.g., Hudson and Cliver, 2001). The estimation of mass in an ejection, from the coronagraph’s view, is relatively straightforward because of the direct dependence of Thomson scattering on n_e . On the other hand, coronagraphs typically have an occulter that precludes any direct observation of contributions from the lower corona. For example, a coronagraph typically does not detect the preflare mass contribution from an erupting filament, one of the principal components of the “three-part” CME structure (Webb and Hundhausen, 1987), and both its mass and any entrained mass below the occulter edge will not have been detected prior to the event.

The emission-line corona, which we observe via EVE spectra, can detect the entire corona, and by differencing, identify that part of the corona that may wind up within a CME. The emission-measure weighting means that we cannot directly estimate a mass from the magnitude of $n_e n_i V$, but additional information would help to resolve this ambiguity. The simplest approach here would be to use the AIA image to determine a projected area A , and thence a crude estimate of the volume as $A^{3/2}$. Then, dimensionally, one can obtain a mean density and therefore a mass. The complexity of the difference images in Figure 2 makes this a difficult approach. Alternatively, a density-diagnostic spectroscopic measurement can also provide some of the missing information (Harrison et al., 2003; Tian et al., 2012). These methods still leave model dependencies (for example, one density-diagnostic line pair cannot describe the physical state of a multithermal plasma well). Tian et al. (2012) in particular found that the emission-line dimming mass could comprise 20–60% of the total CME mass, which seems reasonable but not definitive.

Our dimming temperature estimates reflect the pristine initial state of the CME plasma via its charge-state distribution. In the resulting ICME, in situ particle measurements can also determine the charge-state distribution of Fe, and any differences could result either from plasma dynamics during the CME/ICME evolution after launch, or from the eruption physics itself. Our $\langle T \rangle \approx 1.35$ MK corresponds roughly to $q_{\text{Fe}} = 10$, consistent with the quiet corona but distinctly different from the frequent occurrence of values of $q_{\text{Fe}} \geq 14$ observed in ICMEs (Lepri et al., 2001). The mechanism that causes these differences appears not to be well understood at present. Powerful CMEs normally come from active regions, as did all of the events in our sample. Active-region plasma certainly includes higher temperatures than the diffuse corona does (e.g., Brosius, Daw, and Rabin, 2014), and it seems quite possible that the eruption could incorporate hot material from this source. Our EVE perspective does not presently allow us to resolve this question, which will require careful work with DEM distributions and image data.

4. Conclusions

We have studied a sample of ten dimming events as seen in the EUV emission lines detected by EVE; all had associated flares and CMEs. These Sun-as-a-star dimming observations provide an alternative perspective on the CME phenomenon in general (cf. Hudson and Cliver, 2001): there is no occulting disk, but the inference of physical parameters (mass or temperature) must be EM-weighted, rather than more directly from n_e as with the definitive coronagraphic Thomson-scattering observation. Another limitation of any Sun-as-a-star observation comes from the need to estimate a background level, since we must interpret the emission/dimming signatures as the excess/deficit over this level. For most of our events we could define relatively steady preflare intervals as background references, and thus obtain the dimming deficit in each of a set of emission lines. The difference time series across the EUV spectrum clearly distinguish the flare emission signatures (both impulsive and gradual phases) from the effects of the dimming. For our measurements we took a one-hour event interval, generally near the minimum time of the Fe x 177.23 Å dimming, and a substantially longer background interval. For each we could estimate empirical uncertainties via the bootstrap method. We restricted the analysis to lines with formation temperature below that of Fe IV, as lines at higher temperatures did not always display dimming.

The main results in this study come from the EM-weighted mean temperatures of each event. We found that the preflare reference intervals had substantially higher temperatures than those of the dimming volume alone, as expected from a global Sun usually hosting at

least one active region capable of producing flares and CMEs. Thus, we restricted the EM-weighted sampling to lines with formation temperatures $\log(T/K) < 6.3$. Figure 5 summarizes the essential findings, which we list as:

- The dimming volumes have comparable temperatures to those of the preflare sources (for $\log(T/K) < 6.3$).
- The preflare temperatures strongly agree from event to event, whereas the dimming temperatures have substantial variation.
- There is no appreciable correlation between dimming depth and reference temperature, suggesting that we cannot identify CME-prone active regions based on their EM-weighted temperatures.
- The results are generally consistent with the conclusion that the bulk of the EVE dimming material resided in the general corona, rather than in the active regions themselves.

The scope of our analysis leaves open the interesting question regarding the generation of the high charge states in ICME plasmas (e.g., Lepri et al., 2001). Adiabatic cooling must be overcome by heating and/or ionization as the CME expands; we suggest that more extensive studies of EVE dimming spectroscopy in the context of imaging data may help to explain how this works.

Acknowledgments We thank the School of Physics and Astronomy, University of Glasgow, for support (ET) and hospitality (HH). This research originated in the undergraduate Honours Laboratory course, 2023, under the supervision of Graham Woan and Sargam Mulay, whom we thank for assistance with EVE data and for advice.

Author contributions E.T. wrote the bulk of the text and made most of the figures. Both authors reviewed the manuscript.

Data Availability All data used in this study are in the public domain. The EVE data are accessible through the Virtual Solar Observatory at <https://lasp.colorado.edu/eve/data> and the AIA/HMI images through the Joint Science Operations Center (JSOC) at <http://jsoc.stanford.edu>.

Declarations

Competing interests The authors declare no competing interests.

Open Access This article is licensed under a Creative Commons Attribution 4.0 International License, which permits use, sharing, adaptation, distribution and reproduction in any medium or format, as long as you give appropriate credit to the original author(s) and the source, provide a link to the Creative Commons licence, and indicate if changes were made. The images or other third party material in this article are included in the article's Creative Commons licence, unless indicated otherwise in a credit line to the material. If material is not included in the article's Creative Commons licence and your intended use is not permitted by statutory regulation or exceeds the permitted use, you will need to obtain permission directly from the copyright holder. To view a copy of this licence, visit <http://creativecommons.org/licenses/by/4.0/>.

References

- Brosius, J.W., Daw, A.N., Rabin, D.M.: 2014, Pervasive faint Fe XIX emission from a solar active region observed with EUNIS-13: evidence for nanoflare heating. *Astrophys. J.* **790**, 112. DOI. ADS.
- Efron, B., Tibshirani, R.J.: 1993, *An Introduction to the Bootstrap*, Chapman & Hall, London.
- Hansen, R.T., Garcia, C.J., Hansen, S.F., Yasukawa, E.: 1974, Abrupt depletions of the inner corona. *Publ. Astron. Soc. Pac.* **86**, 500. DOI. ADS.
- Harrison, R.A., Bryans, P., Simnett, G.M., Lyons, M.: 2003, Coronal dimming and the coronal mass ejection onset. *Astron. Astrophys.* **400**, 1071. DOI. ADS.

- Hudson, H.S., Cliver, E.W.: 2001, Observing coronal mass ejections without coronagraphs. *J. Geophys. Res.* **106**, 25199. DOI. ADS.
- Hudson, H.S., Strong, K.T., Dennis, B.R., Zarro, D., Inza, M., Kosugi, T., Sakao, T.: 1994, Impulsive behavior in solar soft X-radiation. *Astrophys. J. Lett.* **422**, L25. DOI. ADS.
- Jin, M., Cheung, M.C.M., DeRosa, M.L., Nitta, N.V., Schrijver, C.J.: 2022, Coronal mass ejections and dimmings: a comparative study using MHD simulations and SDO observations. *Astrophys. J.* **928**, 154. DOI. ADS.
- Lepri, S.T., Zurbuchen, T.H., Fisk, L.A., Richardson, I.G., Cane, H.V., Gloeckler, G.: 2001, Iron charge distribution as an identifier of interplanetary coronal mass ejections. *J. Geophys. Res.* **106**, 29231. DOI. ADS.
- Mason, J.P., Woods, T.N., Caspi, A., Thompson, B.J., Hock, R.A.: 2014, Mechanisms and observations of coronal dimming for the 2010 August 7 event. *Astrophys. J.* **789**, 61. DOI.
- Mason, J.P., Attie, R., Arge, C.N., Thompson, B., Woods, T.N.: 2019, The SDO/EVE solar irradiance coronal dimming index catalog. I. Methods and algorithms. *Astrophys. J. Suppl.* **244**, 13. DOI.
- Pesnell, W., Thompson, B., Chamberlin, P.: 2012, The Solar Dynamics Observatory. *Solar Phys.* **275**, 3. DOI.
- Reinard, A.A., Biesecker, D.A.: 2008, Coronal mass ejection-associated coronal dimmings. *Astrophys. J.* **674**, 576. DOI.
- Rust, D.M.: 1983, In: Roederer, J.G. (ed.) *Coronal Disturbances and Their Terrestrial Effects* **21**, Springer, Dordrecht. ISBN 978-94-009-7096-0. DOI.
- Sterling, A.C., Hudson, H.S.: 1997, Yohkoh SXT observations of X-ray “dimming” associated with a halo coronal mass ejection. *Astrophys. J.* **491**, L55. DOI.
- Tian, H., McIntosh, S.W., Xia, L., He, J., Wang, X.: 2012, What can we learn about solar coronal mass ejections, coronal dimmings, and extreme-ultraviolet jets through spectroscopic observations? *Astrophys. J.* **748**, 106. DOI. ADS.
- Veronig, A.M., Odert, P., Leitinger, M., Dissauer, K., Fleck, N.C., Hudson, H.S.: 2021, Indications of stellar coronal mass ejections through coronal dimmings. *Nat. Astron.* **5**, 697. DOI. ADS.
- Webb, D.F., Hundhausen, A.J.: 1987, Activity associated with the solar origin of coronal mass ejections. *Solar Phys.* **108**, 383. DOI. ADS.
- Woods, T.N., Eparvier, F.G., Hock, R., Jones, A.R., Woodraska, D., Judge, D., Didkovsky, L., Lean, J., Mariska, J., Warren, H., McMullin, D., Chamberlin, P., Berthiaume, G., Bailey, S., Fuller-Rowell, T., Sojka, J., Tobiska, W.K., Viereck, R.: 2012, Extreme ultraviolet variability experiment (EVE) on the solar dynamics observatory (SDO): overview of science objectives, instrument design, data products, and model developments. *Solar Phys.* **275**, 115. DOI. ADS.
- Zarro, D.M., Sterling, A.C., Thompson, B.J., Hudson, H.S., Nitta, N.: 1999, SOHO EIT observations of extreme-ultraviolet “dimming” associated with a halo coronal mass ejection. *Astrophys. J.* **520**, L139. DOI.

Publisher's Note Springer Nature remains neutral with regard to jurisdictional claims in published maps and institutional affiliations.